Changes in primary productivity and chlorophyll *a* in response to iron fertilization in the Southern Polar Frontal Zone

Frank Gervais[1] and Ulf Riebesell

Alfred Wegener Institute for Polar and Marine Research, P.O. Box 12 01 61, D-27515 Bremerhaven, Germany

Maxim Y. Gorbunov

Environmental Biophysics and Molecular Ecology Program, Institute of Marine and Coastal Sciences, Rutgers, The State University of New Jersey, 71 Dudley Road, New Brunswick, New Jersey 08901

Abstract

EisenEx—the second in situ iron enrichment experiment in the Southern Ocean—was performed in the Atlantic sector over 3 weeks in November 2000 with the overarching goal to test the hypothesis that primary productivity in the Southern Ocean is limited by iron availability in the austral spring. Underwater irradiance, chlorophyll *a* (Chl *a*), photochemical efficiency, and primary productivity were measured inside and outside of an iron-enriched patch in order to quantify the response of phytoplankton to iron fertilization. Chl *a* concentration and photosynthetic rate (^{14}C uptake in simulated in situ incubations) were measured in pico-, nano-, and microphytoplankton. Photochemical efficiency was studied with fast repetition rate fluorometry and xenon–pulse amplitude modulated fluorometry. The high-nutrient low-chlorophyll waters outside the Fe-enriched patch were characterized by deep euphotic zones (63–72 m), low Chl *a* (48–56 mg m^{-2}), low photosynthetic efficiency ($F_v/F_m \approx 0.3$), and low daily primary productivity (130–220 mg C m^{-2} d^{-1}). Between 70 and 90% of Chl *a* was found in pico- and nanophytoplankton. During the induced bloom, F_v/F_m increased up to ~0.55, primary productivity and Chl *a* reached the maximum values of 790 mg C m^{-2} d^{-1} and 231 mg Chl *a* m^{-2}, respectively. As a consequence, the euphotic depth decreased to ~41 m. Picophytoplankton biomass hardly changed. Nano- and microphytoplankton biomass increased. In the first 2 weeks of the experiment, when the depth of the upper mixed layer was mostly <40 m, primary productivity was highly correlated with Chl *a*. In the third week, productivity was much lower than predicted from Chl *a,* probably because of a reduction in photosynthetic capacity as a consequence of increased physical variability in the upper water column. These results provide unequivocal evidence that iron supply is the central factor controlling phytoplankton primary productivity in the Southern Ocean, even if the mixing depth is >80 m.

The Antarctic circumpolar current (ACC) is characterized by low phytoplankton biomass and productivity despite high nutrient availability (Tréguer and Jacques 1992; de Baar and Boyd 2000). In situ observations and shipboard mesocosm incubations suggested that besides light and grazing, iron is an important factor controlling phytoplankton productivity

in the ACC (de Baar and Boyd 2000). The first in situ iron-release experiment in the Pacific sector of the Southern Ocean, SOIREE, was conducted in the late austral summer (February 1999) and produced a phytoplankton bloom (Boyd et al. 2000). This experiment followed two in situ iron enrichment experiments (IronEx I and II) performed in another high-nutrient low-chlorophyll (HNLC) region, namely the equatorial Pacific (Martin et al. 1994; Coale et al. 1996).

Iron containing enzymes plays a central role in plant metabolism (Geider and La Roche 1994). The reduction of phytoplankton photosynthesis under low iron supply is due to a combination of different physiological responses, including a reduction in cellular chlorophyll content and a decline in the efficiency of photosynthetic electron transfer (Geider and La Roche 1994; Hutchins 1995). The photosynthetic response of algae to iron limitation is dependent on light conditions (Sunda and Huntsman 1997) and is connected to nitrogen metabolism (Hutchins 1995).

Iron availability influences phytoplankton species composition. As algal iron uptake varies with cell surface area, small algae (mostly picophytoplankton) are favored when ambient iron concentrations are low (Sunda and Huntsman 1997). These algae are controlled by fast-growing microzooplankton grazers (Price et al. 1994). Upon iron enrichment, larger algae (mostly diatoms) become dominant because they cannot be controlled by microzooplankton and have higher growth rates than their crustacean grazers (Geider and La Roche 1994; de Baar and Boyd 2000).

Here, we report the dynamics of light climate, chlorophyll *a* (Chl *a*) concentration, and primary productivity during the in situ iron enrichment experiment, EisenEx, that was conducted in the Atlantic sector of the Southern Ocean in November 2000 (Smetacek 2001). EisenEx has the overarching goal to test the hypothesis that primary productivity in the Southern Ocean is limited by iron availability in the austral spring. The previous experiment, SOIREE, was performed south of the Antarctic Polar Front in the Pacific sector in late austral summer (Boyd et al. 2000). Thus, EisenEx differed from SOIREE not only in the season, but in the place. Another fundamental distinction of EisenEx was the great abundance of grazing copepods (Bathmann et al. 2001), which was about one order of magnitude higher than that in the SOIREE area (Zeldis 2001).

The aim of the present study is to quantify the iron-induced response of primary productivity of different phytoplankton size classes in a water body from the Polar Frontal Zone in austral spring. We measured Chl *a* concentration and ^{14}C uptake in samples taken throughout the water column inside the Fe-enriched water body over a period of 3 weeks. The integral amount of Chl *a* and the areal daily primary productivity were calculated and compared with reference measurements in nonfertilized waters. By determining Chl *a* and photosynthetic parameters (P_m^* and α^*) in different size fractions, we were able to analyze the specific performances of pico-, nano-, and microphytoplankton throughout the induced phytoplankton bloom. As in previous Fe enrichment experiments (Kolber et al. 1994; Behrenfeld et al. 1996; Boyd and Abraham 2001), an iron-induced increase in the photochemical quantum efficiency of phytoplankton was recorded by using fast repetition rate fluorometry (FRRF; Kolber et al. 1998). In addition, this parameter was assessed using a different method, xenon–pulse amplitude modulated (Xe-PAM) fluorometry.

Material and methods

Work at sea—The experiment was performed in the Atlantic sector of the Southern Ocean ($\sim 21°E$, $48°S$) in austral spring (6–29 Nov 2000) during the cruise ANT XVIII/2 of RV *Polarstern*. To ensure reasonably stable hydrographic conditions, a mesoscale eddy (diameter ~ 100–150 km) that originated from the southern Polar Front and had drifted about 400 km northward was chosen as the experimental location (Strass et al. 2001). In the center of the eddy (marked with a drifting buoy), an area of about 50 km^2 was enriched with acidified iron sulfate solution containing the tracer SF_6 (Strass et al. 2001). Iron enrichment was repeated twice, with intervals of 8 d. The overall strategy of the iron fertilization procedure was similar to that employed during IronEx and SOIREE and ensured an increase in iron concentration from the background values (<0.1 nM) up to levels above the saturation of phytoplankton growth (Croot et al. 2001). Sampling and in situ measurements were performed inside and outside of the Fe-enriched water body (''the patch'') throughout the experiment. The position of the sampling stations was selected based on horizontal surveys of the surface SF_6 concentration (Watson et al. 2001). ''In-

stations'' were situated at the highest SF_6 concentrations observed, whereas ''out-stations'' were within waters of the eddy that showed background SF_6 concentrations (Watson et al. 2001). Two of the in-station sampling casts were, in fact, situated at the edge of the Fe-enriched patch because the ship had drifted out of the center of the patch when the respective casts were performed. This was revealed by subsequent analysis of on-line measurements of SF_6 concentration and photochemical efficiency. Samples were collected by a multibottle water sampler (Sea-Bird SBE 32) equipped with 24 bottles (12 liters each), conductivity–temperature–depth (CTD) probes (Sea-Bird Electronics SBE 911plus), and a Haardt fluorometer. Usually samples were taken at 12 different depths between 5 and 200 m.

Irradiance, attenuation coefficient, euphotic depth, mixed layer depth, critical depth—Global radiation was recorded every minute with a Cm11 pyranometer. Downwelling irradiance in air (E_a; PAR, 400–700 nm; see Table 1 for all symbols and abbreviations) was measured every minute with a LI-COR 192SA cosine quantum sensor placed on the ship's helicopter deck (van Oijen pers. comm.). The vertical profiles of underwater downward irradiance (E_d; PAR, 400–700 nm) were measured with a QCD-900L Quantum Cosine Deep Profiling Sensor (Biospherical Instruments) that was installed on the rosette sampler. The vertical attenuation coefficient (k_d) was calculated from the plots of ln E_d versus depth and averaged for four different water layers (10–40, 40–60, 60–80, 80–100 m). Because k_d changed with depth, the euphotic depth (z_{eu}) could not be simply calculated from k_d. Therefore, we calculated subsurface irradiance [$E_d(0)$] from the linear regression of ln $E_{d,10–40m}$ versus depth and read z_{eu} [the depth where $E_d = 1\%$ $E_d(0)$] from the measured data. The depth of the upper mixed layer (z_{uml}) was estimated by visual inspection of all plots of temperature, salinity, and σ_t as the depth of the first clear change in one of these variables. However, there was no universal criterion that could be applied to determine z_{uml}. The critical depth (z_c)—the mixing depth that would result in no net phytoplankton growth—was calculated according to Nelson and Smith (1991) as $z_c = \Sigma E_a/(3.78k_d)$, where ΣE_a is the daily sum of E_a.

Chl a, *phaeopigments, nutrients*—Immediately after sampling, separate 1,000-ml aliquots were filtered on a Whatman GF/F filter (yielding total pigment concentration), a 2.0-μm polycarbonate membrane, and a 20-μm net filter (vacuum differential <300 mbar). The 2.0- and 20-μm filtrates were again filtered through GF/F filters. The filters were ground in 10-ml 90% acetone, extracted at 4°C for 2 h, and centrifuged. The extract fluorescence was measured before and after acidification with 1 N HCl using a Turner Design Model 10-AU digital fluorometer. The concentrations of Chl *a* and phaeopigments were calculated according to Arar and Collins (1992). The size classes were derived from the following samples/calculations: <2 μm, 2-μm filtrate; >20 μm, 20-μm filter; 2–20 μm, total concentration minus 20-μm filter minus 2-μm filtrate.

The concentrations of nitrate, phosphate, and silicate were

Table 1. List of symbols and abbreviations used.

Symbol	Meaning	Units
α	Maximum light utilization coefficient	μg C L^{-1} h^{-1} (μmol photons m^{-2} s^{-1})$^{-1}$
α^*	α normalized to Chl a	μg C (μg Chl a)$^{-1}$ h^{-1} (μmol photons m^{-2} s^{-1})$^{-1}$
ADP	Areal daily primary productivity between 0 and 100 m	mg C m^{-2} d^{-1}
β	Photoinhibition parameter	μg C L^{-1} h^{-1} (μmol photons m^{-2} s^{-1})$^{-1}$
Chl a	Chlorophyll a	
Chl a_{100}	Integral amount of Chl a between 0 and 100 m	mg m^{-2}
Chl a_{zeu}	Integral amount of Chl a between 0 and z_{eu}	mg m^{-2}
E	Irradiance	μmol photons m^{-2} s^{-1}
E_a	Downwelling irradiance in air	μmol photons m^{-2} s^{-1}
E_d	Underwater downwelling irradiance	μmol photons m^{-2} s^{-1}
$E_d(0)$	Downwelling irradiance in subsurface water	μmol photons m^{-2} s^{-1}
E_k	Light saturation parameter ($P_m^*/\alpha^?$)	μmol photons m^{-2} s^{-1}
F_0	Minimum fluorescence level in the dark-adapted state	
F_m	Maximum fluorescence level in the dark-adapted state	
F_v	Maximum variable fluorescence ($F_v = F_m - F_0$)	
F_v/F_m	Potential photochemical efficiency of photosystem II	
k_d	Vertical attenuation coefficient of downwelling irradiance	m^{-1}
P	Photosynthetic rate	μg C L^{-1} h^{-1}
P_m	Maximum photosynthetic rate	μg C L^{-1} h^{-1}
P_m^*	P_m normalized to Chl a	μg C (μg Chl a)$^{-1}$ h^{-1}
P_s	Maximum, potential, light-saturated photosynthetic rate	μg C L^{-1} h^{-1}
PAR	Photosynthetically active radiation	μmol photons m^{-2} s^{-1}
SIS incubation	Simulated in situ incubation	
z_c	Critical depth	m
z_{eu}	Euphotic depth	m
z_{uml}	Upper mixed layer depth	m

determined on board using a Technicon II Autoanalyzer following standard methods.

Primary productivity—Experiments: To analyze the relationship between photosynthetic rate (P) and irradiance (E), we exposed the samples in an incubator designed according to Babin et al. (1994). It consists of incubation chambers placed radially around a strong light source (Osram HQI-T 250 W/D). Up to 19 polystyrene culture flasks (25 cm², 60 ml volume; Corning) can be placed in each chamber. The light gradient in this set of flasks is due to the increasing distance to the light source and to the neutral-density filters placed between some of the flasks. Irradiance was measured inside the culture flasks with a spherical PAR sensor of 6 mm diameter (Zemoko). The temperature of the samples in the flasks was maintained by flushing the incubation chambers with seawater from a depth of 8 m and the addition of ice. The incubator was located in a temperature-controlled (3°C) room.

We applied two different approaches to measure the P versus E relationship. In both approaches, 60 μCi NaH^{14}CO$_3$ (Hartmann Analytic) were added per 60-ml sample of water, and the samples were incubated for 4 h in the flasks of the Babin incubator. To keep algae in suspension, the flasks were gently mixed after 2 h incubation.

In the first P versus E approach, 12 aliquots (60-ml) of a near-surface sample (usually 20 m depth) were incubated at 12 different light intensities (between 1.6 and 1,400 μmol photons m^{-2} s^{-1}), and three aliquots (60-ml) were kept in darkness. After the incubation, three 20-ml subsamples of each flask were filtered on a 0.45-μm cellulose nitrate filter

(Sartorius), a 2.0-μm polycarbonate filter (Nuclepore), and a 20.0-μm polycarbonate filter (Poretics), respectively. Filtration through the 20-μm filter was by gravity, whereas vacuum pressures <200 mbar were applied for the other filter sizes.

The second approach was a simulated in situ incubation (SIS). We used samples from 9–10 depths of the upper 100 m of the water column. For each depth, one 60-ml subsample was incubated at the approximate irradiance that prevailed at sampling depth when a subsurface irradiance of 500 μmol photons m^{-2} s^{-1} was assumed. Additional dark bottles were incubated from four depths. After the incubation, three 20-ml parallel samples of each flask were filtered on 0.45-μm cellulose nitrate filters (Sartorius; vacuum differential <200 mbar).

In both approaches, the filters were washed two times with 1 ml filtered seawater and were then placed on a filter paper soaked with 0.1 N HCl to release unassimilated ^{14}CO$_2$. After adding scintillation cocktail (3.5 ml Packard Filter Count per filter), the activity on the filters was counted at sea in a Packard Tricarb1900 TR scintillation counter. Quench correction was done using internal standard additions. The photosynthetic rate (P) was calculated according to standard procedures (Strickland and Parsons 1968) on the basis of simultaneously measured concentrations of TCO$_2$ (de Baar pers. comm.).

Calculations: To describe the P versus E relationship, we followed the recommendations of Frenette et al. (1993). We employed the exponential function of Webb et al. (1974) (Eq. 1) to describe the P versus E curves without photo-

inhibition and the exponential function of Platt et al. (1980) (Eqs. 2a,b) when photosynthesis was inhibited at higher irradiance levels.

$$P = P_m \cdot [1 - \exp(-\alpha \cdot E/P_m)] \tag{1}$$

$$P = P_s \cdot [1 - \exp(-\alpha \cdot E/P_s)] \cdot [\exp(-\beta \cdot E/P_s)] \tag{2a}$$

$$P_m = P_s \cdot [\alpha/(\alpha + \beta)] \cdot [\beta/(\alpha + \beta)]^{\beta/\alpha} \tag{2b}$$

These models were also applied to the results of simulated in situ incubations. It should be noted that this approach yields a P versus E relationship that is a composite of the photosynthetic performances of algae having different irradiance histories (Henley 1993). The models were fit to the experimental data with the use of the software Origin (OriginLab Corporation), which calculates the fitting curve and standard errors for parameter estimates in an iterative process based on the Marquardt–Leevenberg nonlinear least squares fitting algorithm. The results of the first P versus E approach gave a good fit to the model chosen (mostly Eq. 1) with a mean $r^2 = 0.980$ and a minimum $r^2 = 0.918$. The SIS data were described with Eq. 2, with a mean $r^2 = 0.985$ and a minimum $r^2 = 0.948$.

To estimate areal daily primary productivity (ADP), we first calculated subsurface irradiance $[E_d(0)]$ from downwelling irradiance in air (E_a) in 5-min intervals on each sampling day $[E_d(0) = 0.75621E_a$; Bracher et al. (1999)]. From $E_d(0)$ and the vertical attenuation coefficients (k_d) (*see above*), we calculated PAR at 15 depths between 0 and 100 m. Photosynthetic rate was calculated with Eq. 1 from the resulting PAR and from the parameter estimates of the Webb model (Eq. 1) fitted to the results of the respective SIS incubations. To derive ADP, we integrated photosynthetic rate over depth (15 depths) and time (5-min intervals) for each day. To quantify the mean daily irradiance available for phytoplankton photosynthesis (mean E_d), we averaged PAR over depth (from 0 m to z_{eu} or from 0 m to z_{uml} if $z_{uml} > z_{eu}$) and time (between sunrise and sunset).

To determine the photosynthetic parameters of the P versus E relationships of the different phytoplankton size classes (total phytoplankton, >0.45 μm; picophytoplankton, 0.45–2 μm; nanophytoplankton, 2–20 μm; microphytoplankton, >20 μm), we first estimated the model parameter estimates from the photosynthetic rate data of the three filtered size fractions (>0.45, >2, >20 μm). Based on these parameters, we subsequently computed the modeled P versus E curves of the three size fractions and calculated the P versus E curves of the phytoplankton size classes from these curves. Finally, we normalized these curves to the Chl a concentration and calculated the respective model parameters.

Photochemical efficiency—The potential photochemical efficiency of photosystem II (F_v/F_m) of phytoplankton was assessed by using a xenon–pulse amplitude modulated (Xe-PAM) fluorometer (Walz) (Schreiber et al. 1993) and a fast repetition rate (FRR) fluorometer. In the first case, samples were dark adapted at ambient temperature for 60 min. Unconcentrated subsamples were transferred to a cuvette in the center of the fluorometer optical unit ED-101 US/M (Walz)

and again dark adapted for 5 min. For the measurement of F_0 and F_m, one measuring flash (Xe-MF, Walz) was triggered right before and one right after the saturation pulse (Xe-AL, Walz). Fluorescence was detected with the photodiode detector (Xe-PD, Walz) and processed with specially designed software. In each subsample, these measurements were repeated 10 times at 30-s intervals and averaged. The results were corrected by subtracting the background fluorescence of 0.2-μm filtered subsamples. The Xe-PAM fluorometer was placed in a temperature-controlled (3°C) room. The custom-built FRR fluorometer and measurement protocols are described by Kolber et al. (1998).

Results

Temperature, light, vertical mixing, and nutrient conditions—During the period of investigation (6–29 Nov 2000), water temperature increased from 3.5 to 4.2°C near the surface and from 2.0 to 3.5°C at 100 m depth. Day length increased from 15 to 16 h. Daily global radiation varied between 4.9 and 27.1 MJ m^{-2} d^{-1}, with values below 10 MJ m^{-2} d^{-1} for only 7 of the 24 d.

The vertical attenuation coefficient of downward irradiance $(k_{d,10-40m})$ was between 0.070 and 0.083 m^{-1} outside the Fe-enriched patch, but gradually increased to 0.114 m^{-1} inside the patch (Fig. 1A). $k_{d,10-40m}$ was linearly correlated with the sum of concentrations of Chl a and phaeopigments (Phaeo) in the upper 40 m ($k_{d,10-40m} = 0.0176$[Chl a + Phaeo] + 0.0633; $r = 0.877$, $n = 52$, $p < 0.0001$). The euphotic depth (z_{eu}) remained roughly constant (67 $\pm$ 3.5 m) outside the patch but steadily decreased to 41 m inside the patch (Fig. 1B).

The depth of the upper mixed layer (z_{uml}) was highly variable during the experiment. z_{uml} was mostly <40 m during the first 2 weeks and increased to >80 m during the last week of the experiment. This increase in mixing depth and light attenuation resulted in a distinct increase in the ratio of z_{uml} to z_{eu} (Fig. 1C).

On six sampling days with low daily sums of downwelling irradiance (mean $\Sigma E_a = 20.5 \pm 7.2$ mol photons m^{-2} d^{-1}), the critical depth (z_c) was <100 m (Fig. 1D). On most other sampling days, ΣE_a was much higher (mean $\Sigma E_a = 45.5 \pm 6.9$ mol photons m^{-2} d^{-1}) and z_c exceeded 100 m (Fig. 1D). During the third week of the experiment, z_c was larger outside than inside the patch (Fig. 1D) because of higher underwater light attenuation in the patch (Fig. 1A). Except for day 9, z_c significantly exceeded z_{uml}.

The depth-averaged daily mean irradiance (mean E_d) was between 100 and 150 μmol m^{-2} s^{-1} on most sampling days (inside and outside the patch; data not shown). Only on the 6 d with $z_c < 100$ m (Fig. 1D) and on the last in-station, the mean E_d was between 38 and 80 μmol m^{-2} s^{-1}. On the last day of our observations (day 21: $z_{uml} = 80$ m, $\Sigma E_a = 45.7$ mol photons m^{-2} d^{-1}) mean E_d was 66 μmol m^{-2} s^{-1} inside the patch and 100 μmol m^{-2} s^{-1} outside.

The lowest nutrient concentrations measured at any depth between 0 and 100 m outside the patch were 22 μM nitrate, 1.6 μM phosphate, and 10 μM silicate. Inside the patch, major nutrients were still abundant on day 21 of the exper-
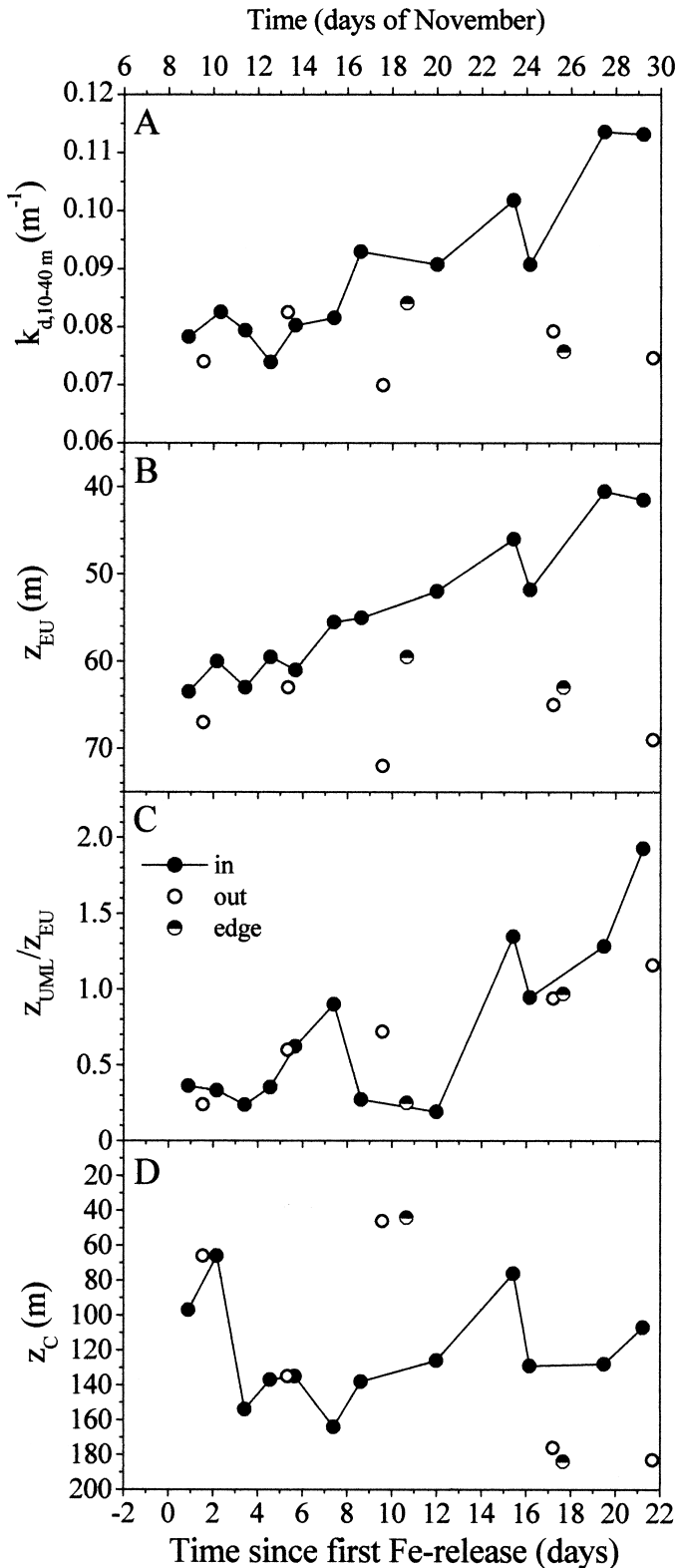
Fig. 1.   Temporal evolution of (A) the vertical attenuation coefficient of downward irradiance ($k_{d,10-40m}$), (B) euphotic depth (z_{eu}), (C) the ratio of the depth of the upper mixed layer (z_{uml}) to euphotic depth, and (D) the critical depth (z_c) inside and outside of the Fe-enriched water body during the experiment. Two stations were at the edge of the Fe-enriched patch.

iment (>20 μM nitrate, >1.5 μM phosphate, >10 μM silicate; mean values of the upper 100 m).

Chl a—The areal amount of Chl *a* (Chl a_{100}) remained between 48 and 56 mg m^{-2} outside the Fe-enriched patch (Fig. 2A). The maximum Chl *a* concentration observed at any depth of the upper 100 m remained constant ($\sim$0.60 mg m^{-3}) outside the patch. Inside the patch, Chl a_{100} started to increase from the background level 4 d after the first iron infusion and reached the maximum value of 231 mg m^{-2} on day 21 (Fig. 2A). Outside the Fe-enriched patch, the percentage of Chl *a* in picophytoplankton (<2 μm) was 28–39% (Fig. 2B). The percentage of Chl *a* in nanophytoplankton was 42–52% (2–20 μm) and in microphytoplankton was 9–30% (>20 μm; i.e., 0.05–0.17 mg Chl *a* m^{-3}) (Fig. 2B). Inside the patch, the percentage of Chl *a* in nanophytoplankton decreased slightly—from about 50 to 44%—and that in picophytoplankton more drastically—from 42 to 13%. In contrast, Chl *a* in microphytoplankton increased from 10 to 43% in the course of the experiment (Fig. 2C). In absolute numbers, Chl *a* in picophytoplankton slightly increased from 0.2 to 0.3 mg m^{-3} in the first week and remained roughly constant thereafter, whereas Chl *a* in nano- and microphytoplankton increased from 0.25 to 1.1 mg m^{-3} and from 0.05 to 1.1 mg m^{-3}, respectively (Fig. 2D).

The in-station increase in Chl *a* concentration was restricted to the upper 50–60 m in the first 2 weeks. Because of the deepening of the upper mixed layer, however, the algal bloom extended to more than 80 m in the third week (Fig. 3). The relative contribution of different size classes to total Chl *a* showed only minor variations with depth (not shown).

Areal daily primary productivity—The integrated primary productivity was between 130 and 220 mg C m^{-2} d^{-1} outside the Fe-enriched patch (Fig. 4A). Inside the patch, primary productivity started to increase on day 2, reached the maximum of 790 mg C m^{-2} d^{-1} on day 16, and decreased thereafter (Fig. 4A). The low values of primary productivity at the out-station and the edge-station on days 9 and 10 (Fig. 4A) were due to the unusually low global radiation on these days (31 and 37% of the mean daily radiation during the experiment (i.e., 4.9 and 5.9 MJ m^{-2} d^{-1}). Nanophytoplankton contributed between 13 and 34% to primary productivity both inside and outside the Fe-enriched patch (Fig. 4B,C). Picophytoplankton was always the most important primary producer outside the patch (Fig. 4B) and at least for the first 2 weeks inside the patch (Fig. 4C). The percentage of primary productivity by microphytoplankton varied between 10 and 38% outside (Fig. 4B). Inside the patch, microphytoplankton became the dominant producer (>50%) at the end of the observation period (Fig. 4C).

The assimilation rate (ADP normalized to Chl a_{100}) increased from 4 to 7 mg C (mg Chl a_{100})$^{-1}$ d^{-1} inside the patch during the first and second week of the experiment (Fig. 5A). In the third week—when the ratio z_{uml}/z_{eu} had increased (Fig. 1D) and the amount of Chl *a* below the euphotic zone increased (*see next paragraph*)—the in-station assimilation rate decreased even below the level of the out-stations (Fig. 5A). When ADP was normalized to chlorophyll in the euphotic zone (Fig. 5B), the in-station assimi-
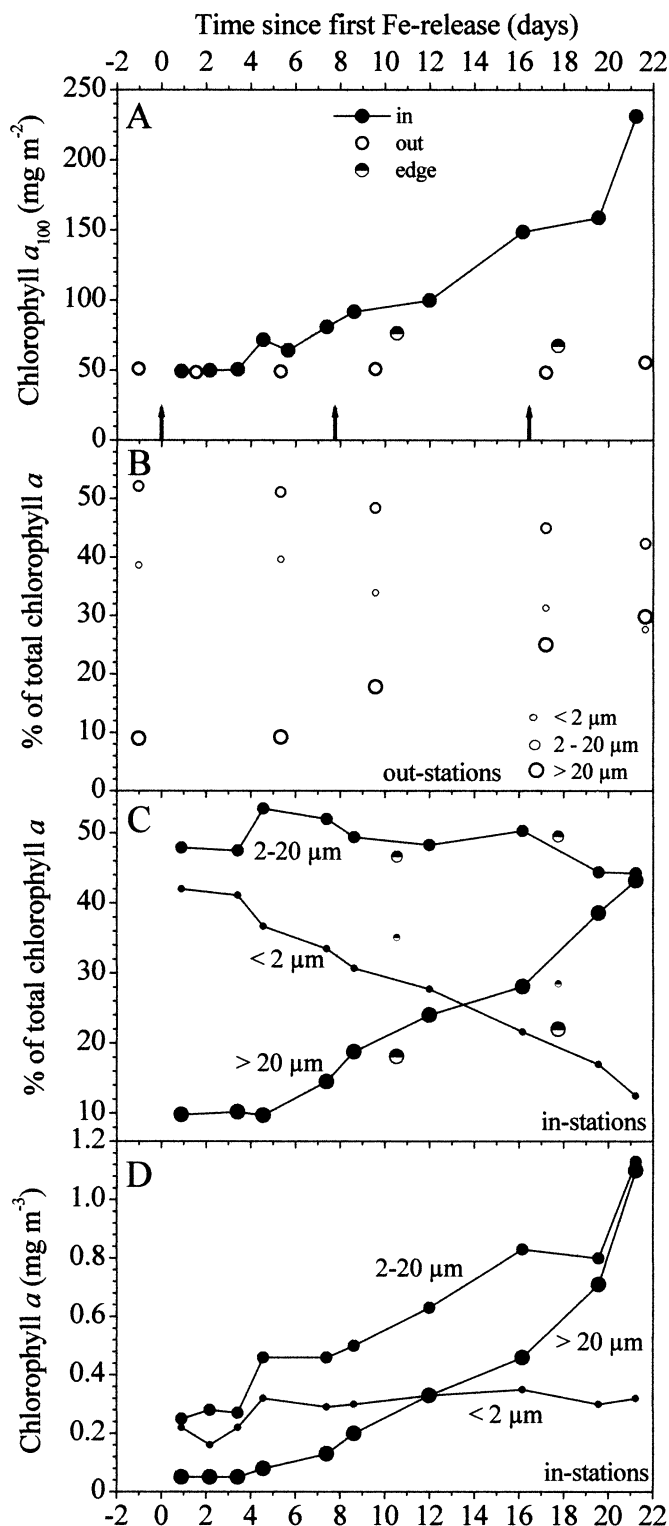
Fig. 2. (A) Areal amount of Chl *a* inside and outside of the Fe-enriched patch during the experiment (integral between 0 and 100 m depth). (B, C) Temporal development of the relative contribution of three different phytoplankton size classes to the total Chl *a* concentration (means of all measurements between 0 and 80 m) outside (B) and inside (C) the Fe-enriched patch. (D) Chl *a* concentration of three different phytoplankton size classes (mean between 0 and 80 m depth). The arrows at the bottom of panel (A) mark the times of the three iron infusions. The half-filled symbols (in A, C) refer to the stations located at the edge of the patch.
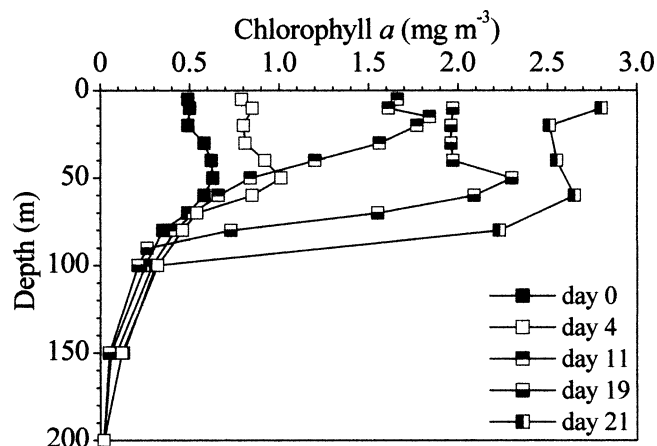

Fig. 3. Vertical distribution of the Chl *a* concentration inside the Fe-enriched patch on five exemplary days.

lation rate increased in the first week, reached maximum values of around 9–10 mg C (mg Chl a_{zeu})$^{-1}$ d^{-1} in the second week and decreased below the initial values in the last week. The low assimilation rates on days 9 and 10 (Fig. 5A,B) were due to the low global radiation on these days (*see above*).

Predicting ADP inside the patch—ADP inside the patch correlated best with the areal amount of Chl a_{100} during the first 12 d of the experiment (linear correlation: ADP = 9.36 Chl a_{100} − 238.0; $n = 7$; $r^2 = 0.984$; $p < 0.0001$). On days 16, 19, and 21, a large percentage of Chl a_{100} was found below z_{eu} (39, 50, and 53%, respectively). ADP during the first 16 d could be predicted with the highest significance when correlated with Chl a_{zeu} (Fig. 5C). ADP measurements made on days 19 and 21 could not, however, be sensibly included in regression analysis either versus Chl a_{100} (not shown) or versus Chl a_{zeu} (marked with "1" in Fig. 5C). When all in-station ADP measurements were considered, correlation analysis revealed much lower levels of significance (ADP vs. Chl a_{100}: $r^2 = 0.299$, $n = 10$, $p = 0.102$; ADP vs. Chl a_{zeu}: $r^2 = 0.581$, $n = 10$, $p = 0.010$). The inclusion of incoming irradiance in regression analysis (by plotting ADP of all in-stations vs. Chl $a \cdot \Sigma E_a$) did not result in a higher significance. Four of the ADP versus Chl a_{zeu} measurements made outside and at the edge of the patch also came close to the regression line for the in-station data (Fig. 5C). The out- and edge-station measurements on days 9 and 10 (marked with "2" in Fig. 5C) revealed very low ADP in comparison to Chl a_{zeu} because these days had the lowest global radiation (*see preceding paragraph*). The results of the last out-station (marked "3" in Fig. 5C) also did not fit into the in-station trend.

P versus E relationships—The parameters characterizing the P versus E relationship of total phytoplankton in the near-surface samples were rather variable (Fig. 6). Both P_m^* and α^* showed an overall decrease, especially at the end of the observation period (Fig. 6A,B). P_m^* was between 0.7 and 2.1 μg C (μg Chl *a*)$^{-1}$ h^{-1} and did not show distinct differences inside and outside the Fe-enriched patch (Fig. 6A). α^*
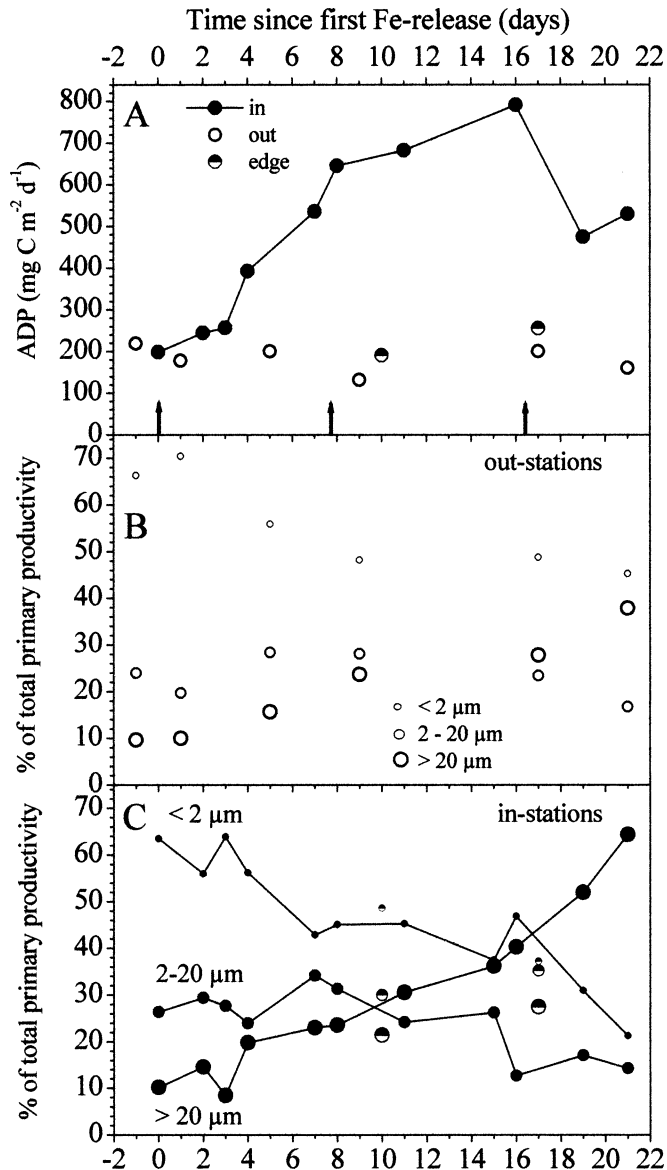
Fig. 4. (A) Areal daily primary productivity inside and outside of the Fe-enriched patch during the experiment. (B, C) Temporal development of the relative contribution of three different phytoplankton size classes to total primary productivity in a near-surface sample (usually from 20 m depth) outside (B) and inside (C) the Fe-enriched patch. The arrows at the bottom of panel A mark the times of the three iron infusions. The half-filled symbols (in A, C) refer to the stations located at the edge of the patch.

was between 0.006 and 0.016 μg C (μg Chl a)$^{-1}$ h^{-1} (μmol photons m^{-2} s^{-1})$^{-1}$ (Fig. 6B). Outside the patch, α^* was at the lower edge of this range, never exceeding values of 0.013 (Fig. 6B). Except at four dates, E_k ranged between 103 and 128 μmol photons m^{-2} s^{-1} (Fig. 6C).

P_m^* and α^* of pico-, nano-, and microphytoplankton inside the patch were clearly different (Fig. 7A,B), whereas the E_k ranges of the three size classes overlapped between 32 and 190 μmol photons m^{-2} s^{-1} (not shown). P_m^* and α^* were lowest in nanophytoplankton, intermediate in microphytoplankton, and highest in picophytoplankton (Fig. 7A,B). P_m^*

and α^* of nano- and microphytoplankton varied in rather narrow ranges, whereas the P versus E parameters of picophytoplankton scattered over a larger range and partly overlapped with the microphytoplankton parameter range (Fig. 7A,B).

Photochemical efficiency—While measured with the Xe-PAM fluorometer, the potential photochemical efficiency of photosystem II (F_v/F_m) in phytoplankton outside the Fe-enriched patch was in the range of 0.23–0.28 (Fig. 8A). Inside the patch, F_v/F_m was around 0.30 during the first days of the experiment and increased to 0.45 on day 21 (Fig. 8A).

The FRRF-derived values of F_v/F_m showed similar patterns both outside and inside the patch (Fig. 8B) but were always ~25% higher than the Xe-PAM–derived numbers. In the near-surface phytoplankton, the FRRF-derived F_v/F_m remained constant in nonfertilized waters (~0.30), but increased dramatically inside the patch (Fig. 8B). At depth (>40 m), F_v/F_m values were usually ~20–30% higher than at the surface (data not shown), suggesting the reduction in the extent of nutrient limitation with depth. Deconvolution analysis of the high-resolution pattern of F_v/F_m (Fig. 8B) revealed three waves in the iron-mediated increase of F_v/F_m that were driven by the iron infusions (arrows in Fig. 8B). The maximum values of F_v/F_m measured by FRRF in the iron-enriched patch were as high as 0.55 to 0.56 during the last week of EisenEx.

Discussion

EisenEx—the second mesoscale in situ iron-enrichment experiment in the Southern Ocean—was successful in inducing a marked phytoplankton bloom in the austral spring and was able to follow the development of the bloom over a period of 3 weeks. We observed a maximum primary productivity of 790 mg C m^{-2} d^{-1} inside the patch compared to ~200 mg C m^{-2} d^{-1} outside. At the end of the observation period (day 21), phytoplankton biomass in the center of the Fe-enriched patch had increased considerably, as was evident by a more than fourfold rise in Chl a concentration.

The development of the algal bloom was strongly influenced by physical processes. Wind speeds during the first and second weeks of our experiment were distinctly lower than the seasonal average values in this region (Dentler 2001). As a consequence, z_{uml} seldom exceeded 40 m. A storm on days 13 and 14 resulted in complete mixing of the upper 80 m of the water column. With alternate periods of medium and strong wind (Dentler 2001), the mixing conditions during the third week of the experiment were typical for the ACC (Mitchell et al. 1991). Because of horizontal dispersion, the patch of elevated Chl a concentration had enlarged to an area of about 500 km^2 on day 17/18 of the experiment (Riebesell unpubl. data). Despite the heavy storms encountered, the very center of the patch probably was only slightly diluted by horizontal dispersion as was indicated by steadily increasing values of F_v/F_m at the in-stations. Very likely, changes in the extent of vertical mixing were the dominant physical factor influencing the development of the phytoplankton in the center of the patch.

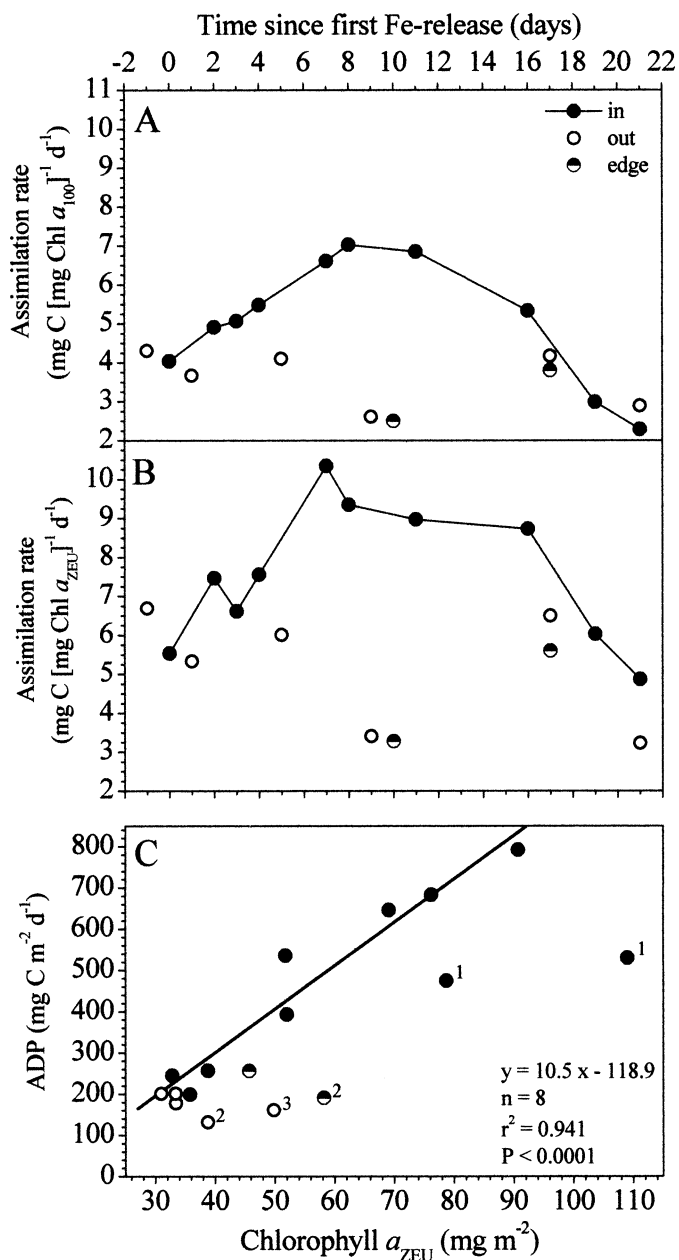The EisenEx in situ experiment was comparable to a nat-

Fig. 5. (A, B) Assimilation rate inside and outside of the Fe-enriched patch during the experiment. (A) ADP was normalized to Chl a_{100}. (B) ADP was normalized to Chl a_{zeu}. (C) ADP versus Chl a_{zeu}. The line and parameters in panel B result from linear regression analysis of the in-station results (excluding the two data points from days 19 and 21 marked with "1"). The data in panel C marked with "2" were measured on days with very low global radiation (days 9 + 10); the data point marked with "3" represents the out-station measurement on day 21.
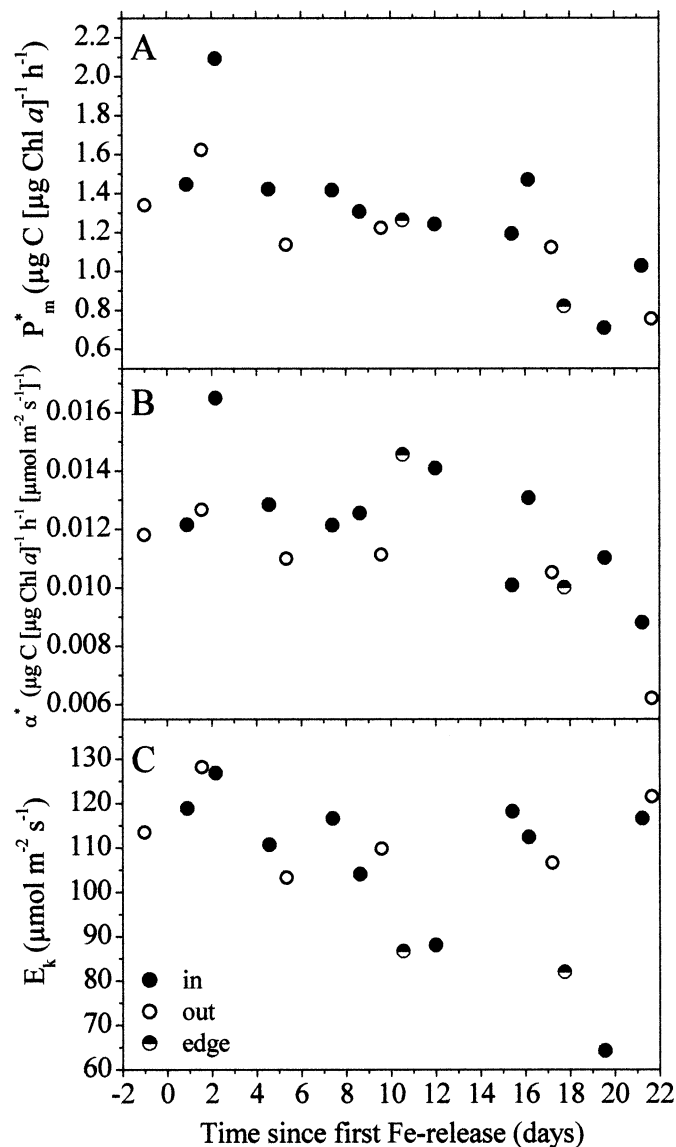

Fig. 6. Parameters of the P versus E relationships of total phytoplankton in near-surface samples at the stations inside, outside, and at the edge of the Fe-enriched patch during the experiment.

ural iron fertilization event investigated in the Polar Frontal region in the austral spring of 1992 (Smetacek et al. 1997). The exceptionally high iron concentrations encountered in the Polar Frontal Zone (de Baar et al. 1995) are suggested to be due to the iron release from abundant icebergs present in the area in spring 1992 (Smetacek et al. in press). Under conditions of shallow mixed layers, distinct phytoplankton blooms with maximum primary productivity between 1,000 and 3,000 mg C m^{-2} d^{-1} (Jochem et al. 1995) were present in the iron-enriched waters.

Photochemical efficiency—Our results show that, similar to FRR fluorometry (Falkowski and Kolber 1995; Kolber et al. 1998), Xe-PAM fluorometry (Schreiber et al. 1993) is sufficiently sensitive to characterize phytoplankton photochemistry in oligotrophic ocean regions. During EisenEx, both techniques revealed the iron-stimulated increase in F_v/F_m. The underestimation of F_v/F_m by the Xe-PAM fluorometer requires further investigation.

F_v/F_m responded to the iron addition with a slight but distinct increase within a day. This is because the Fe-dependent synthesis of key components of photosystem II is very rapid (Falkowski and Kolber 1995). Such a fast increase was ob-
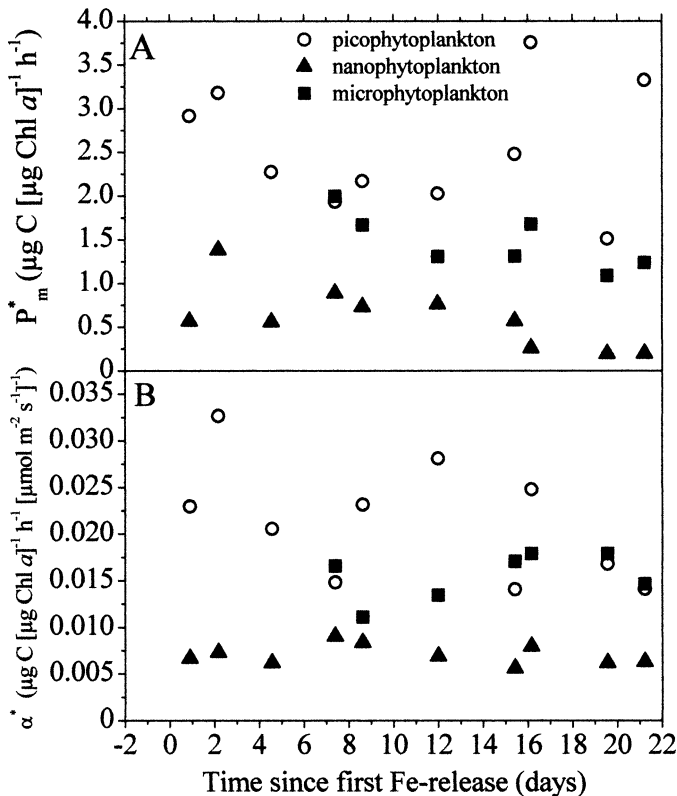
Gervais et al.

Fig. 7. Temporal evolution of the parameters of the P versus E relationships of pico-, nano-, and microphytoplankton in near-surface samples at the stations inside the Fe-enriched patch. The parameters of the microphytoplankton are missing on the first three sampling days because they could be reliably normalized only when the Chl *a* concentration of this size fraction was >0.08 μg L^{-1}.

Fig. 8. (A) Temporal evolution of the potential photochemical efficiency of photosystem II (F_v/F_m) measured by the Xe-PAM fluorometer at the stations inside, outside, and at the edge of the Fe-enriched patch. The graph shows the mean ± 1 SD of five samples taken between 20 and 60 m depth. (B) Dynamics of F_v/F_m recorded by the FRR fluorometer in near-surface phytoplankton inside and outside the patch. The arrows at the bottom of panel B mark the times of the three iron infusions.

served in all prior Fe enrichment experiments and has been interpreted as unequivocal evidence for a physiological stimulation of the phytoplankton by Fe addition (Kolber et al. 1994; Behrenfeld et al. 1996; Boyd and Abraham 2001).

The quantitative assessment of the extent of nutrient limitation requires the accurate knowledge of reference parameters for nutrient-replete phytoplankton communities in the area. The values of F_v/F_m for nutrient-replete phytoplankton in the area of EisenEx were precisely determined in the shipboard nutrient enrichment incubation experiments (not shown) and were 0.57 ± 0.01 for the single turnover FRR protocol and 0.68 ± 0.02 for the multiple turnover protocol (analogous to PAM). The values of F_v/F_m measured in the iron-fertilized patch during the last week of EisenEx were only ~5% lower than these reference numbers, clearly suggesting that the iron infusions have fully eliminated the iron stress and that iron was the major limiting nutrient in the area. A suboptimal iron supply cannot be excluded, however, because under deteriorating iron conditions, different compensatory mechanisms are applied before F_v/F_m will eventually be reduced (McKay et al. 1997; Boyd et al. 2000). Maldonado et al. (2001) revealed a set of physiological adaptations that allow phytoplankton in Southern Ocean HNLC waters to adapt to shifts in iron speciation, explaining the long-lasting maintenance of iron-induced blooms.
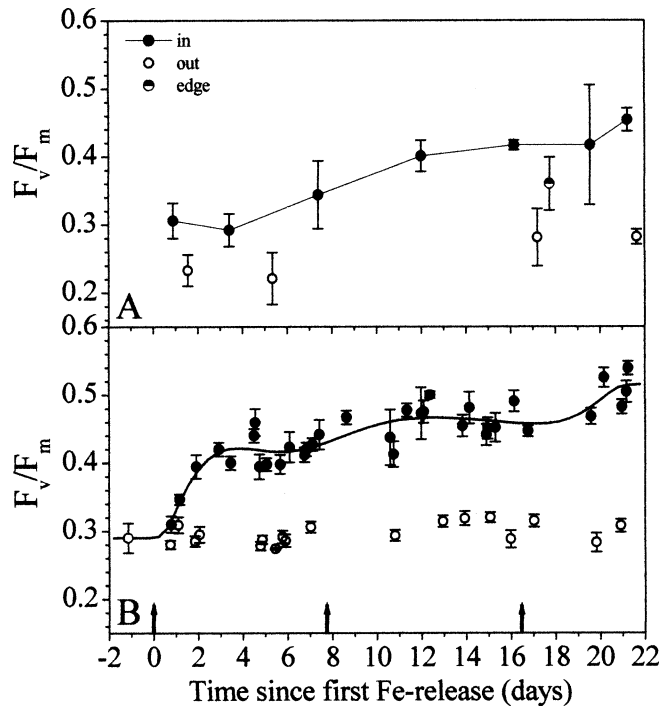
P versus E parameters—During IronEx I, phytoplankton inside the Fe-enriched patch showed an increase in P_m^* and α^* (Kolber et al. 1994). P_m^* in Fe-replete cultures of *Phaeodactylum tricornutum* doubled in comparison with Fe-deficient cultures, whereas α^* was slightly lower (Greene et al. 1991). During EisenEx, we observed no general inside/outside difference in P_m^*, whereas α^* was slightly higher inside the Fe-enriched patch. These deviating trends might be due to the different phytoplankton species involved. In general, the results indicate an iron-induced rise in photosynthetic performance that is in accordance with the observed increase in photochemical efficiency.

The values of P_m^*, α^*, and E_k measured in the present study are well within the wide range found in Southern Ocean phytoplankton (Sakshaug and Slagstad 1990; Bracher et al. 1999). Because the stations were made at different times of the day, part of the variability observed might be due to diel cycles in photosynthetic parameters (Prézelin 1992). The low values of P_m^* at the end of the observation period might have been a response to the large changes in z_{uml} because phytoplankton communities have been shown to exhibit reduced P_m^* in a physically variable environment (Harris et al. 1980). The decreasing percentage of picophytoplankton biomass, which was characterized by a relatively high P_m^*, could also have contributed to a decreasing bulk phytoplankton P_m^*.

The obvious differences in P_m^* and α^* between pico-,

nano-, and microphytoplankton (Fig. 7) can be attributed to differences in algal cellular size and surface/volume ratio, respectively. The effectiveness of a pigment molecule in absorbing photons is generally larger for smaller cells because of the reduced package effect (Raven 1999). This leads to a larger α^* in picophytoplankton because this parameter is a measure of the efficiency of light use (Joint and Pomroy 1986; Geider and Osborne 1992). Higher P_m^* in picophytoplankton cells might have been a consequence of their superior performance in terms of resource acquisition and use (Raven 1999). P_m^* and α^* should decrease with increasing cell size as long as the concentration of pigment in the cell is independent of cell size. Accordingly, P_m^* and α^* were distinctly lower in nanophytoplankton than in picophytoplankton. The P versus E parameters of the largest size class—the microphytoplankton—were, however, intermediate. This might be explained by the observation that species of the pennate diatom genus *Pseudo-nitzschia,* characterized by a rather favorable surface/volume ratio, were codominating the microphytoplankton inside the patch (Assmy and Henjes unpubl. data).

Chl a *and primary productivity in the surrounding HNLC waters*—Outside the patch, typical HNLC conditions prevailed. Major nutrients were always abundant, but the mean Chl a concentration was constrained between 0.48 and 0.56 mg m^{-3} in the upper 100 m. In the Atlantic sector of the Southern Ocean, primary productivity in the range of 130–220 mg C m^{-2} d^{-1}, as observed during our study, has also been measured by Jochem et al. (1995) in the ACC in October/November 1992 and by Bracher et al. (1999) between the southern Polar Front and the northern ACC in December/January 1995/1996. Froneman et al. (2001) reported an ADP between 60 and 266 mg C m^{-2} d^{-1} south of and within the Antarctic Polar Front (Atlantic sector) in January/February 1993. Parallel to the investigations of Jochem et al. (1995), Detmer and Bathmann (1997) observed that pico- and nanophytoplankton contributed more than 70–80% to total Chl a when Chl a concentration was <0.6 mg m^{-3}. The same was obviously true during EisenEx. An HNLC region in the western Pacific sector of the Southern Ocean is also dominated by pico- and nanophytoplankton and exhibits the same range of ADP as that observed in the present study (Chiba et al. 2000; Strutton et al. 2000). The results of our observations qualify the out-stations as appropriate reference sites for the in situ Fe-enrichment experiment.

Chl a *and primary productivity during the induced bloom*—Nelson and Smith (1991) predicted from critical depth–mixing depth relationships that a maximum Chl a concentration of only ~1 mg m^{-3} can be realized in Southern Ocean surface waters even if all (macro- and micro-) nutrients are sufficient. Observations and modeling of the Antarctic phytoplankton crop in relation to mixed layer depth led Mitchell et al. (1991) to the conclusion that a substantial increase in phytoplankton biomass is only possible when $z_{uml} < 40$–50 m. These hypothesis could not be tested by SOIREE because the mixing depth declined from an initial 65 m to 20–40 m in the course of that experiment (Boyd et al. 2000). The present study revealed, however, that iron

fertilization is able to produce higher Chl a levels (mixed layer mean 2.6 mg m^{-3}) even if $z_{uml} > 80$ m. This was mainly because of the favorable incident PAR (mean $\Sigma E_a = 34.2 \pm 13.7$ mol photons m^{-2} d^{-1}). Severe light limitation due to heavy cloud cover played a role only on a few days throughout the whole period of observation.

Nevertheless, the increase in z_{uml} observed in the course of the present study did influence the underwater light climate and the photosynthetic performance of phytoplankton. Inside the patch, the substantial reduction of the euphotic depth due to the increased algal biomass and the increase in z_{uml} during the third week of the experiment reduced the distance between the critical depth and z_{uml} to about 30 m at favorable global radiation conditions. The varying wind conditions in the third week of our observations very likely induced frequent short-term changes in z_{uml}. This had the consequence that periods when a considerable portion of the phytoplankton was trapped below the euphotic zone alternated with periods when phytoplankton was exposed to high ratios of mixed layer depth to euphotic depth. This physically variable environment was probably the most important factor responsible for the observed reduction in P_{max} (Fig. 6A; cf. Harris et al. 1980) and for the distinct decrease in the assimilation rate (Fig. 5B) outside and especially inside the Fe-fertilized patch. Notwithstanding, receiving a daily mean E_d of 66 μmol photons m^{-2} s^{-1} inside the patch, the Fe-induced phytoplankton bloom was still growing on day 21 when the ship was scheduled to leave the experimental area.

In the course of SOIREE, primary productivity showed a stronger increase (from ~100 to ~1,400 mg C m^{-2} d^{-1} within 13 d; Gall et al. 2001*b*) compared to the present study (from ~200 to ~700 mg C m^{-2} d^{-1} within 13 d) despite lower Chl a concentrations. The assimilation rates therefore were clearly higher during SOIREE (Gall et al. 2001*b*). The assimilation rates measured during SOIREE and EisenEx were, however, within the wide range observed in the Southern Ocean (Jochem et al. 1995), and future studies should address the question of whether the observed differences were due to differences in phytoplankton species composition or different degrees of iron limitation.

Following an increase in F_v/F_m on day 1 and an increase in primary productivity on day 2, Chl a in pico-, nano-, and microphytoplankton started to rise 4 d after the EisenEx iron infusion. Whereas picophytoplankton showed no further buildup in biomass (in terms of Chl a), nano- and microphytoplankton biomass increased continuously at almost equal rates until day 16. In the following days, microphytoplankton showed the strongest increase, subsequently catching up with nanophytoplankton. This change in phytoplankton community structure agrees well with the expected response to the relaxation of iron limitation. Comparable trends have been observed in all Fe-related in situ observations, shipboard mesocosm experiments, and in situ experiments (Cavender-Bares et al. 1999; de Baar and Boyd 2000; Chiba et al. 2000; Gall et al. 2001*a*). These trends are in accordance with the "ecumenical" iron hypothesis (Cullen 1995), which assumes the control of picoplankton by fast-growing microzooplankton and iron-stimulated growth of larger phytoplankton that is unchecked by slowly growing

mesozooplankton. The observations made during IronEx II and SOIREE, however, revealed that the underlying food web interactions are much more complicated (Landry et al. 2000; Rollwagen Bollens and Landry 2000; Hall and Safi 2001). Moreover, it is important to recognize that the response in phytoplankton structure and productivity observed in the beginning of an iron-induced bloom might only be transient and that the response to prolonged iron supply remains to be elucidated.

References

ARAR, E. J., AND G. B. COLLINS. 1992. Method 445.0—in vitro determination of Chl *a* and phaeophytin *a* in marine and freshwater phytoplankton by fluorescence, p. 1–14. *In* US EPA methods for the determination of chemical substances in marine and estuarine environmental samples. U.S. Environmental Protection Agency.

BABIN, M., A. MOREL, AND R. GAGNON. 1994. An incubator designed for extensive and sensitive measurements of phytoplankton photosynthetic parameters. Limnol. Oceanogr. **39:** 694–702.

BATHMANN, U., S. SCHULTES, AND S. KRÄGEFSKY. 2001. Zooplankton work during "EisenEx". Ber. Polarforsch. Meeresforsch. **400:** 215–221.

BEHRENFELD, M. J., A. J. BALE, Z. S. KOLBER, J. AIKEN, AND P. G. FALKOWSKI. 1996. Confirmation of iron limitation of phytoplankton photosynthesis in the equatorial Pacific Ocean. Nature **383:** 508–511.

BOYD, P. W., AND E. R. ABRAHAM. 2001. Iron-mediated changes in phytoplankton photosynthetic competence during SOIREE. Deep-Sea Res. II **48:** 2529–2550.

———, AND OTHERS. 2000. A mesoscale phytoplankton bloom in the polar Southern Ocean stimulated by iron fertilization. Nature **407:** 695–702.

BRACHER, A. U., B. M. A. KROON, AND M. I. LUCAS. 1999. Primary production, physiological state and composition of phytoplankton in the Atlantic sector of the Southern Ocean. Mar. Ecol. Prog. Ser. **190:** 1–16.

CAVENDER-BARES, K. K., E. L. MANN, S. W. CHISHOLM, M. E. ONDRUSEK, AND R. R. BIDIGARE. 1999. Differential response of equatorial Pacific phytoplankton to iron fertilization. Limnol. Oceanogr. **44:** 237–246.

CHIBA, S., AND OTHERS. 2000. An overview of the biological/oceanographic survey by the RTV *Umitaka-Maru III* off Adelie Land, Antarctica in January–February 1996. Deep-Sea Res. II **47:** 2589–2613.

COALE, K. H., AND OTHERS. 1996. A massive phytoplankton bloom induced by an ecosystem-scale iron fertilization experiment in the equatorial Pacific Ocean. Nature **383:** 495–501.

CROOT, P., AND OTHERS. 2001. Iron fertilization in the Atlantic sector of the Southern Ocean. Ber. Polarforsch. Meeresforsch. **400:** 133–148.

CULLEN, J. J. 1995. Status of the iron hypothesis after the Open-Ocean Enrichment Experiment. Limnol. Oceanogr. **40:** 1336–1343.

DE BAAR, H. J. W., AND P. W. BOYD. 2000. The role of iron in plankton ecology and carbon dioxide transfer of the global oceans, p. 61–140. *In* R. B. Hanson, H. W. Ducklow, and J. G. Field [eds.], The changing ocean carbon cycle. Cambridge Univ. Press.

———, J. T. M. DE JONG, D. C. E. BAKKER, B. M. LÖSCHER, C. VETH, U. BATHMANN, AND V. SMETACEK. 1995. Importance of iron for plankton blooms and carbon dioxide drawdown in the Southern Ocean. Nature **373:** 412–415.

DENTLER, F.-U. 2001. Meteorologische Bedingungen. Ber. Polarforsch. Meeresforsch. **400:** 67–72.

DETMER, A. E., AND U. V. BATHMANN. 1997. Distribution patterns of autotrophic pico- and nanoplankton and their relative contribution to algal biomass during spring in the Atlantic sector of the Southern Ocean. Deep-Sea Res. II **44:** 299–320.

FALKOWSKI, P. G., AND Z. KOLBER. 1995. Variations in chlorophyll fluorescence yields in phytoplankton in the world oceans. Aust. J. Plant Physiol. **22:** 341–355.

FRENETTE, J.-J., S. DEMERS, L. LEGENDRE, AND J. DODSON. 1993. Lack of agreement among models for estimating the photosynthetic parameters. Limnol. Oceanogr. **38:** 679–687.

FRONEMAN, P. W., R. K. LAUBSCHER, AND C. D. MCQUAID. 2001. Size-fractionated primary production in the south Atlantic and Atlantic sectors of the Southern Ocean. J. Plankton Res. **23:** 611–622.

GALL, M. P., P. W. BOYD, J. HALL, K. A. SAFI, AND H. CHANG. 2001*a*. Phytoplankton processes. Part 1: Community structure during the Southern Ocean Iron Release Experiment (SOIREE). Deep-Sea Res. II **48:** 2551–2570.

———, R. STRZEPEK, M. MALDONADO, AND P. W. BOYD. 2001*b*. Phytoplankton processes. Part 2. Rates of primary production and factors controlling algal growth during the Southern Ocean Iron Release Experiment (SOIREE). Deep-Sea Res. II **48:** 2571–2590.

GEIDER, R. J., AND J. LA ROCHE. 1994. The role of iron in phytoplankton photosynthesis and the potential of iron-limitation of primary productivity in the sea. Photosynth. Res. **39:** 275–301.

———, AND B. A. OSBORNE. 1992. Algal photosynthesis. Chapman and Hall.

GREENE, R. M., R. J. GEIDER, AND P. G. FALKOWSKI. 1991. Effect of iron limitation on photosynthesis in a marine diatom. Limnol. Oceanogr. **36:** 1772–1782.

HALL, J. A., AND K. SAFI. 2001. The impact of in situ Fe fertilisation on the microbial food web in the Southern Ocean. Deep-Sea Res. II **48:** 2591–2613.

HARRIS, G. P., G. D. HAFFNER, AND B. P. PICCININ. 1980. Physical variability and phytoplankton communities: II. Primary productivity by phytoplankton in a physically variable environment. Arch. Hydrobiol. **88:** 393–425.

HENLEY, W. J. 1993. Measurement and interpretation of photosynthetic light-response curves in algae in the context of photoinhibition and diel changes. J. Phycol. **29:** 729–739.

HUTCHINS, D. A. 1995. Iron and the marine phytoplankton community. Prog. Phycol. Res. **11:** 1–49.

JOCHEM, F. J., S. MATHOT, AND B. QUÉGUINER. 1995. Size-fractionated primary production in the open Southern Ocean in austral spring. Polar Biol. **17:** 39–53.

JOINT, I. R., AND A. J. POMROY. 1986. Photosynthetic characteristics of nanoplankton and picoplankton from the surface mixed layer. Mar. Biol. **92:** 465–474.

KOLBER, Z. S., AND OTHERS. 1994. Iron limitation of phytoplankton photosynthesis in the equatorial Pacific Ocean. Nature **371:** 145–149.

———, O. PRASIL, AND P. G. FALKOWSKI. 1998. Measurements of variable chlorophyll fluorescence using fast repetition rate techniques: Defining methodology and experimental protocols. Biochem. Biophys. Acta **1367:** 88–106.

LANDRY, M. R., J. CONSTANTINOU, M. LATASA, S. L. BROWN, R. R. BIDIGARE, AND M. E. ONDRUSEK. 2000. Biological response to iron fertilization in the eastern equatorial Pacific (IronEx II). III. Dynamics of phytoplankton growth and microzooplankton grazing. Mar. Ecol. Prog. Ser. **201:** 57–72.

MALDONADO, M. T., AND OTHERS. 2001. Iron uptake and physiological response of phytoplankton during a mesoscale Southern Ocean iron enrichment. Limnol. Oceanogr. **46:** 1802–1808.

MARTIN, J. H., AND OTHERS. 1994. Testing the iron hypothesis in ecosystems of the equatorial Pacific Ocean. Nature **371:** 123–129.

McKAY, R. M. L., R. J. GEIDER, AND J. LaROCHE. 1997. Physiological and biochemical response of the photosynthetic apparatus of two marine diatoms to Fe stress. Plant Physiol. **114:** 615–622.

MITCHELL, B. G., E. A. BRODY, O. HOLM-HANSEN, C. McCLAIN, AND J. BISHOP. 1991. Light limitation of phytoplankton biomass and macronutrient utilization in the Southern Ocean. Limnol. Oceanogr. **36:** 1662–1677.

NELSON, D. M., AND W. O. SMITH, JR. 1991. Sverdrup revisited—critical depths, maximum chlorophyll levels, and the control of Southern Ocean productivity by the irradiance-mixing regime. Limnol. Oceanogr. **36:** 1650–1661.

PLATT, T., C. L. GALLEGOS, AND W. G. HARRISON. 1980. Photoinhibition of photosynthesis in natural assemblages of marine phytoplankton. J. Mar. Res. **38:** 687–701.

PRÉZELIN, B. B. 1992. Diel periodicity in phytoplankton productivity. Hydrobiologia **238:** 1–35.

PRICE, N. M., B. A. AHNER, AND F. M. M. MOREL. 1994. The equatorial Pacific Ocean: Grazer-controlled phytoplankton populations in an iron-limited ecosystem. Limnol. Oceanogr. **39:** 520–534.

RAVEN, J. A. 1999. Picophytoplankton. Prog. Phycol. Res. **13:** 33–106.

ROLLWAGEN BOLLENS, G. C., AND M. R. LANDRY. 2000. Biological response to iron fertilization in the eastern equatorial Pacific (IronEx II). II. Mesozooplankton abundance, biomass, depth distribution and grazing. Mar. Ecol. Prog. Ser. **201:** 43–56.

SAKSHAUG, E., AND D. SLAGSTAD. 1990. Light and productivity of phytoplankton in polar marine ecosystems: A physiological view. Polar Res. **10:** 69–85.

SCHREIBER, U., C. NEUBAUER, AND U. SCHLIWA. 1993. PAM fluorometer based on medium-frequency pulsed Xe-flash measuring light: A highly sensitive new tool in basic and applied photosynthesis. Photosynth. Res. **36:** 65–72.

SMETACEK, V. 2001. EisenEx: International team conducts iron experiment in Southern Ocean. U.S. JGOFS Newsl. **11:** 11–14.

————, H. J. W. DE BAAR, U. V. BATHMANN, K. LOCHTE, AND M. M. RUTGERS VAN DER LOEFF. 1997. Ecology and biogeochemistry of the Antarctic Circumpolar Current during austral spring: A summary of Southern Ocean JGOFS cruise ANT X/6 of R.V. *Polarstern.* Deep-Sea Res. II **44:** 1–21.

————, C. KLAAS, S. MENDEN-DEUER, AND T. A. RYNEARSON. In press. Mesoscale distribution of dominant diatom species relative to the hydrographical field along the Antarctic Polar Front. Deep-Sea Res. II.

STRASS, V., H. LEACH, B. CISEWSKI, S. GONZALEZ, J. POST, V. DA SILVA DUARTE, AND F. TRUMM. 2001. The physical setting of the Southern Ocean iron fertilisation experiment. Ber. Polarforsch. Meeresforsch. **400:** 94–130.

STRICKLAND, J. D. H., AND T. R. PARSONS. 1968. A practical handbook of seawater analysis. Bull. Fish. Res. Board Can. **167:** 266–278.

STRUTTON, P. G., F. B. GRIFFITHS, R. L. WATERS, S. W. WRIGHT, AND N. L. BINDOFF. 2000. Primary productivity off the coast of East Antarctica (80–150°E): January to March 1996. Deep-Sea Res. II **47:** 2327–2362.

SUNDA, W. G., AND S. A. HUNTSMAN. 1997. Interrelated influence of iron, light and cell size on marine phytoplankton growth. Nature **390:** 389–392.

TRÉGUER, P., AND G. JACQUES. 1992. Dynamics of nutrients and phytoplankton, and fluxes of carbon, nitrogen and silicon in the Antarctic Ocean. Polar Biol. **12:** 149–162.

WATSON, A., M.-J. MESSIAS, L. GOLDSON, I. SKJELVAN, P. NIGHTINGALE, AND M. LIDDICOAT. 2001. SF_6 measurements on EisenEx. Ber. Polarforsch. Meeresforsch. **400:** 76–79.

WEBB, W. L., M. NEWTON, AND D. STARR. 1974. Carbon dioxide exchange of *Alnus rubra*: A mathematical model. Oecologia **17:** 281–291.

ZELDIS, J. 2001. Mesozooplankton community composition, feeding, and export production during SOIREE. Deep-Sea Res. II **48:** 2615–2634.